Flow Regimes and Mixing of Dissimilar Fluids in T-Jets Mixers

DOI:
10.1002/ceat.202100536

Document Version
Accepted author manuscript

Margarida S.C.A. Brito[1]

Cláudio P. Fonte[2]

Madalena M. Dias[1]

José Carlos B. Lopes[1,3]

Ricardo J. Santos[1, *]

Flow Regimes and Mixing of Dissimilar Fluids in T-Jets Mixers

Efficient mixing conditions for similar fluids in T-Jets mixers have been well-established. This paper extends the characterization of the mixing of dissimilar fluids. Planar Laser Induced Fluorescence images were captured using fluids with a viscosity ratio between 1.2 and 3. Flow visualizations showed that best mixing conditions are achieved when the jets are well-balanced, and the onset of a chaotic flow regime is determined by the Reynolds number of the more viscous fluid ($\mathrm{Re}_{\mathrm{HJet}} > 100$). CFD simulations were also performed to get deeper insight into the flow field and mixing dynamics, enabling the prediction of the impingement point position. An analytical model based on jets' kinetic energy rate balance is proposed as a design tool to predict the impingement point position.

Keywords: Computational fluid dynamics, Dissimilar fluids, Laminar flow, Mixing, T-jets mixer

Author affiliations

[1]Laboratory of Separation and Reaction Engineering–Laboratory of Catalysis and Materials (LSRE-LCM),
Faculdade de Engenharia, Universidade do Porto, Rua Dr. Roberto Frias, 4200-465 Porto, Portugal.

[2]Department of Chemical Engineering and Analytical Science, The University of Manchester, Oxford Road, Manchester M13 9PL, United Kingdom.

[3]CoLAB NET4CO2, Rua Júlio de Matos, 828-882, 4200-355 Porto, Portugal.

Email corresponding author: rsantos@fe.up.pt

1 Introduction

T-jets mixers were introduced for chemical reaction processes two decades ago [1-3]. T-jets consist of two opposed channels from where two jets issue into a perpendicular channel. Generally, the perpendicular channel is placed directly below the inlet channels and has a width approximately twice the inlets [1-9]. For this configuration, the main flow regimes identified and reported in the literature are stratified, vortex, and engulfment flow regimes [2]. In the stratified flow regime, the two liquid streams flow from the inlet to the outlet, without being mixed by dynamic structures. Vortex and engulfment flow regimes are based on the generation of Dean vortices with a rotation axis in the same direction as the mixing chamber plane symmetry. A detailed description of these regimes and transition mechanisms is given in previous works based on experimental results [5, 6, 8-12] and CFD simulations [1, 2, 4, 7]. Mixing studies for these T-jets mixers have also considered mixing of dissimilar fluids [13-16]. These reactors have been used successfully on the controlled production of nanomaterials [17-19].

A new flow regime in T-jets, the chaotic flow regime, has been confirmed independently by two research groups [20-23]. The main conditions to operate at the chaotic flow regime are the following design changes from the classic T-jets configuration:

- expansion ratios from inlet channel to mixing chamber larger than 4;
- a minimum depth larger than half the mixing chamber width;
- a headspace in the mixing chamber over the inlet channels inception point.

Efficient mixing in the chaotic flow regime occurs above a critical Reynolds number, typically $\mathrm{Re} > 100$ for mixing of similar fluids with water-like properties [20]. The chaotic flow regime consists of the shedding of a vortex street from the impact point of opposed jets towards the outlet. The strong dynamics of mixing promoted by the dynamic evolution of counter-rotating vortices promotes fast mixing [24, 25]. To date, there are no works reported in the scientific literature on the mixing of dissimilar fluids or different flow rates for chaotic flow regimes. This work is the first study of the conditions to onset chaotic flow regimes in T-jets mixers for dissimilar fluids. Planar Laser Induced Fluorescence (PLIF) imaging of mixing in T-jets for different flow rate ratios and viscosities enables the determination of these conditions. A clear relationship is established between the location of the impact point (IP) of the opposed jets and the operation at chaotic flow regimes, with similar conclusions to those obtained for Confined Impinging Jets [26, 27]. Afterwards, the flow is analyzed from CFD simulations to assess the impact of asymmetric flow conditions of the inlet jets on the IP location. An analytical model based on kinetic energy rate balance is proposed for the description of the IP location. This model is assessed from comparison to CFD data.

2 Experimental conditions

2.1 Experimental set-up

The T-Jets mixer set-up used in the study was described in detail in Krupa et al. [24], Krupa et al. [25]. Figure 1 shows a schematic representation, photos of the experimental set-up and a drawing with the mixer geometry. The reagents solutions are delivered from two pressurized stainless-steel tanks (1 in Figure 1) to the T-Jets reactor (4 in Figure 1). Each line has a volumetric flow rate controller (2 in Figure 1) from Alicat Scientific model LC-200CCM-D and a needle valve (3 in Figure 3). For high viscosity ratios, the flow rate achieved from Alicat Scientific flow controllers is not enough to obtain the full range of working conditions in this work. In the experiments with a high viscous liquid stream, a Mini Cori-flow M15 is used to control the flow rate of the more viscous liquid stream. The uncertainty associated to the flow controllers both for Alicat Scientific model LC-200CCM-D and Mini Cori-flow M15 is $\pm 0.2\%$ of flow rate.

Then, two liquid streams are fed to each injector of a T-Jets mixer inserted in an acrylic mono-block. Three T-jets mixer geometries are used, all having a headspace of $h = 2\ \mathrm{mm}$, and the remaining dimensions are:

- W6w1e4 – chamber width $W = 6\ \mathrm{mm}$, inlet jets width $w = 1\ \mathrm{mm}$, and depth $e = 4\ \mathrm{mm}$;
- W6w1e2 – chamber width $W = 6\ \mathrm{mm}$, inlet jets width $w = 1\ \mathrm{mm}$, and depth $e = 2\ \mathrm{mm}$;
- W2w1e4 – chamber width $W = 2\ \mathrm{mm}$, inlet jets width $w = 1\ \mathrm{mm}$, and depth $e = 4\ \mathrm{mm}$;

The mixing mechanisms in T-Jets mixers are studied from PLIF images, whose experimental set-up is also illustrated in Figure 1. The laser sheet illuminates the cross-plane of the mixing chamber (number 6 in Figure 1), and an image is captured by a PIVcam camera from TSI (number 7 in Figure 1). Rhodamine 6G was used as a dyed in this work. Sultan et al. [20] pointed out an ideal concentration of rhodamine of approximately $4 \times 10^{-4}\ \mathrm{gL^{-1}}$, which is within the linear relationship between concentration and fluorescence.

The main operational parameters are the jets Reynolds number and flow rate ratio between jets. The jets Reynolds number is defined as

$$\mathrm{Re}_{i,\mathrm{Hjet}} = \frac{\rho_i v_{\mathrm{inj},i} d_{\mathrm{Hjet},i}}{\mu_i} \quad (1)$$

where i is the jet indices 1 or 2, $v_{\mathrm{inj},i}$ is the surface velocity at the inlet channel, $d_{\mathrm{Hjet},i}$ is the hydraulic diameter of the inlet channel, and ρ_i and μ_i are the density and viscosity, respectively. The flow rate ratio is given by

$$r_s = \frac{q_1}{q_2} \quad (2)$$

where q_1 and q_2 are the flow rates at inlet channels 1 and 2, respectively. Jets 1 and 2 are identified in Figure 3.

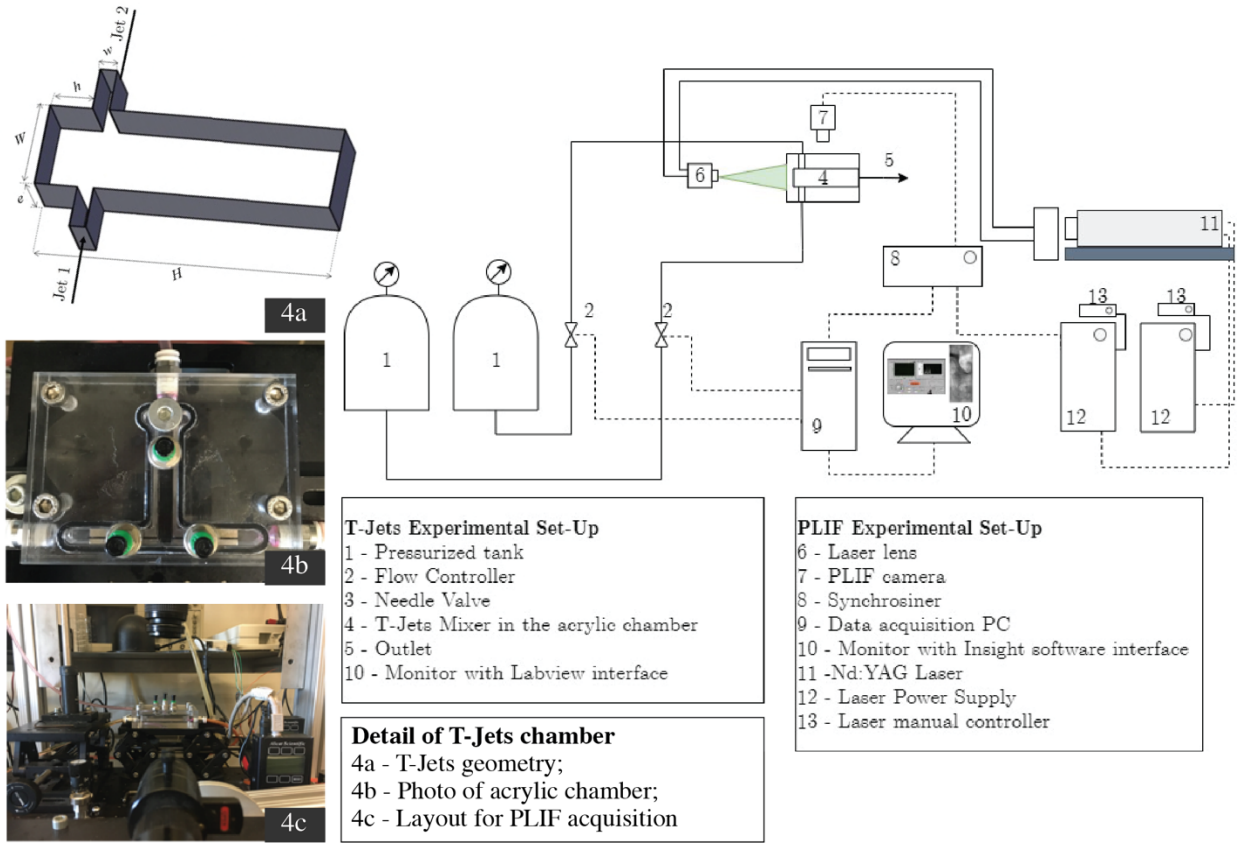

Figure 1. T-jets experimental set-up and mixer geometry.

2.2 Working fluids

The mixing of similar liquids with $\mu = 1.7\ \mathrm{mPa \cdot s}$ and $\rho = 1051\ \mathrm{kg\ m^{-3}}$ is used as the base case for the comparison with the other cases (Case 0 in Table 1). Mixing of similar fluids in T-Jets mixers has been well-established experimentally by Hoffmann et al. [5], Soleymani et al. [6] and Sultan et al. [20], where fluids with water properties were used as model fluids. Glycerol solutions are also used in this work with a viscosity ratio 1.2, considered to perceive whether an offset of 20% on the viscosity in one of the streams has an impact on the mixing dynamics (Case 1). A viscosity ratio of 3 is finally tested, and the mixing dynamics are reported from PLIF images (Case 2).

The glycerol solutions were designed according to the method proposed in Brito et al. [28] for refractive index matching, which is essential for PLIF images of flows with two fluids to minimize reflection, refraction and diffraction. The first step is measuring the refractive index of the more viscous aqueous solution of glycerol, MV fluid. Then, the less viscous fluid, LV fluid, is prepared, and $\mathrm{CaCl_2}$ is added to match the refractive index. Figure 2 shows the changes in refractive index and viscosity of two aqueous solutions of glycerol by adding $\mathrm{CaCl_2}$. Solutions in Figure 2 have viscosities, before adding $\mathrm{CaCl_2}$, $\mu_0 = 1.53\ \mathrm{mPa \cdot s}$ and $\mu_0 = 3.46\ \mathrm{mPa \cdot s}$. The viscosity of the final

solutions was checked in a rheometer Anton Paar MCR 92 SN8247897 and the refractive index was measured at 25 ˚C using a digital ABBE Refractometer (AB-R-100D). The viscosity of streams, the refractive index, and the respective concentration of calcium chloride are listed in Table 1.

Table 1. Sets of fluids for mixing experiments in T-Jets

Case	Viscosity Ratio	μ	ρ	θ [°C]	$C_{CaCl_2 \cdot 2H_2O}$ [kg m^{-3}]	*RI*
0	1:1	$1.7\ \mathrm{mPa \cdot s}$	$1051\ \mathrm{kg\ m^{-3}}$	25	-	-
1	1.2:1	$\mu_{MV} = 1.7\ \mathrm{mPa \cdot s}$ $\mu_{LV} = 1.4\ \mathrm{mPa \cdot s}$	$\rho_{MV} = 1046\ \mathrm{kg\ m^{-3}}$ $\rho_{LV} = 1170\ \mathrm{kg\ m^{-3}}$	22	172	1.41
2	3:1	$\mu_{MV} = 4.1\ \mathrm{mPa \cdot s}$ $\mu_{LV} = 1.4\ \mathrm{mPa \cdot s}$	$\rho_{MV} = 1105\ \mathrm{kg\ m^{-3}}$ $\rho_{LV} = 1257\ \mathrm{kg\ m^{-3}}$	22	259	1.39

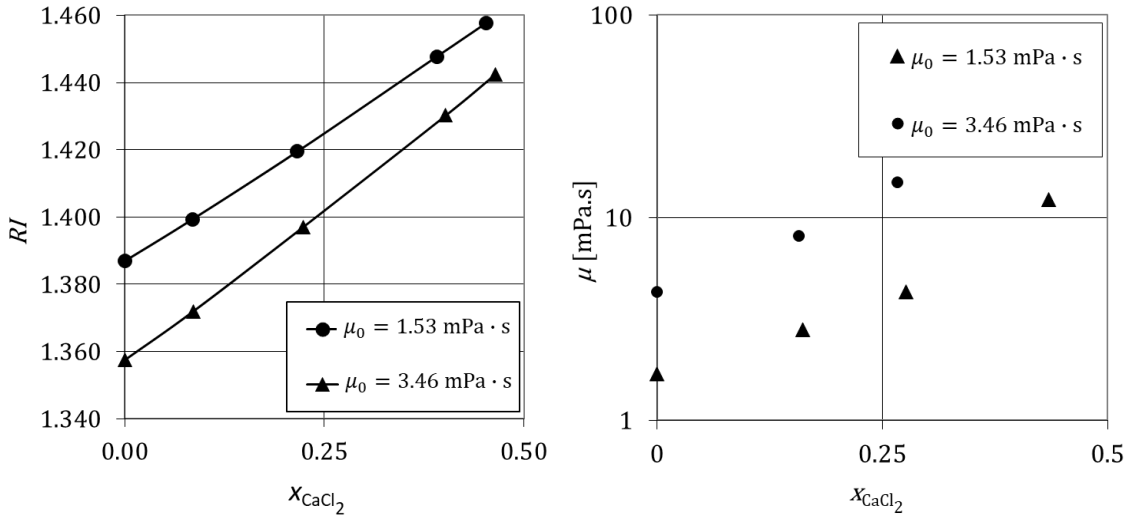

Figure 2. Variation of refractive index and viscosity with the mass fraction of $CaCl_2$.

3 Experimental Results

The analysis of experimental results is divided into three sections: the effect of Reynolds number on mixing of similar fluids; the effect of Reynolds number on mixing of dissimilar fluids, and the impact of imbalance flow conditions on mixing of dissimilar fluids. In the first two sections, balance flow conditions are considered, i.e. when the impingement point position is at the symmetry plane of the mixing chamber. In the third section, asymmetric flow conditions are studied to assess the impact on shifting the jets' impingement point position. The effects of injectors' width, chamber's width and depth are also scrutinized in the following sections.

3.1 Effect of Reynolds number on mixing of similar fluids

Figure 3 shows the concentration field in a plane at the cross-section defined by the mixing chamber and injectors' plane symmetry at conditions of Case 0 for two geometries (W6w1e4 and W6w1e2). The fluid stream injected from jet 1 was dyed with rhodamine emitting fluorescence in the presence of a laser, and thus its color is captured from the PLIF images as white. The dark fluid corresponds to the clear fluid. The image in Figure 3 shows the steady symmetric flow regime where the two fluids flow without convective mixing (W6w1e2 at $\mathrm{Re_{Hjet}} = 119$). For a larger Reynolds number, $\mathrm{Re_{Hjet}} = 395$, it is observed the formation of flow patterns that promote the engulfment of two liquid streams. The flow symmetry is broken when an engulfment flow regime is achieved. This flow regime has been previously identified and thoroughly characterized by several authors [2-6]. This engulfment flow regime is best imaged from the top of the mixing

chamber, as reported in Mariotti et al. [10]. That plane was not captured in this work since the top of the mixing chamber is made of stainless steel, not enabling the flow visualization.

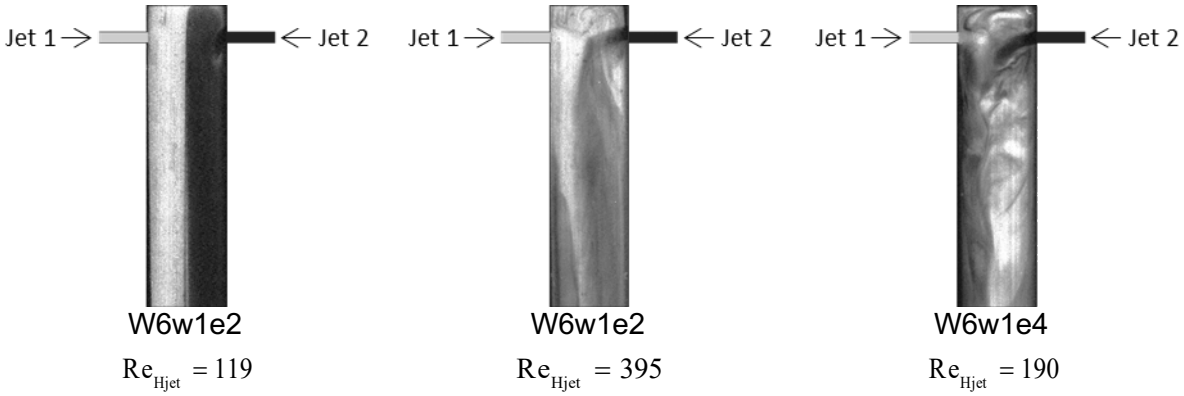

Figure 3. PLIF images in T-jets reactors W6w1e2 and W6w1e4, for $\mu_1 = \mu_2 = 1.7\ \mathrm{mPa \cdot s}$.

Sultan et al. [20] shows that it is not possible to observe the chaotic flow regime for any condition in W2w1e2 geometry. The same conclusion was reported for the tested conditions, as summarized in Table 2.

This work focuses on the less studied chaotic flow regime [20-24, 29], which is best imaged from a front view. This flow is characterized by a vortex street shedding from the impingement point of the opposed jets, as shown in Figure 3 (W6w1e4 at $\mathrm{Re_{Hjet}} = 190$). This flow regime requires that the Reynolds number is above a critical value around 100, and some design particularities: a headspace over the injectors, an expansion from inlet to mixing chamber of at least 4 ($W/w > 4$), and depth larger than half the width ($e > W/2$). The tilting of the jets' interface has also been observed with similar fluids [30]. According to Li et al. [30], the onset of the impingement point position is determined by injectors' velocity profile and the jets' Reynolds number. A similar chaotic flow regime was first identified for Confined Impinging Jets (CIJs), setting two necessary operational conditions: the jets Reynolds number should be above 120, and the opposed jets had to be balanced [26-28]. For T-jets mixers, the issue of the opposed jets balancing and mixing fluids with dissimilar properties or at different flow rates remains unexplored for chaotic flow regimes.

3.2 Effect of Reynolds number on mixing of dissimilar fluids

Figure 4 shows the mixing of two dissimilar fluids, with viscosity ratio $\mu_1/\mu_2 = 1.2$. The MV fluid is injected from the left-hand side injector, jet 1, and the LV fluid is injected from the right-hand side reactor, jet 2 (definition of jets 1 and 2 is in Figure 3). For the W6w1e4 geometry at $\mathrm{Re_{Hjet1}} = 50$ and $\mathrm{Re_{Hjet2}} = 114$, the flow patterns are characteristic of the steady engulfment flow regime. The two inlet streams are engulfed through Dean vortices, the mixing mechanism for vortex or engulfment flow regimes. The rotation axis of the Dean vortices is in the direction of the mixing chamber symmetry plane, and so they are best imaged in cross-sectional views of the flow. Front images of engulfment and vortex flow regimes were previously analyzed in literature [3, 4, 7-9, 11, 31, 32].

At $\mathrm{Re_{Hjet1}} = 500$ and $\mathrm{Re_{Hjet2}} = 514$ for W6w1e4, a self-sustainable chaotic flow regime is generated. The formation of a vortex street that engulfs both inlet streams is clear in Figure 4. This result shows, for the first time, the possibility to promote chaotic flow regimes in T-jets mixers for dissimilar fluids.

The same study was made for the other geometries, W2w1e2 and W6w1e2. For the narrower geometry ($W = 2\mathrm{mm}$), chaotic flow regimes were not attained for fluids with different viscosities, similarly to the observations made for similar fluids [20]. In T-jets mixers with smaller expansion ratios (W/w), the flow is generally in vortex regime [20]. For the shallower chamber with $e = 2\mathrm{mm}$ and the expansion ratio of $W/w = 6$, the chaotic regime is also not so clear. Although the flow

shows some dynamic mixing patterns, the vortices rotation axis is not so markedly perpendicular to the main flow direction as in a purely chaotic flow regime. This phenomenon was scrutinized from fully resolved 3D CFD simulations for the mixing of similar fluids showing the same behaviour [33].

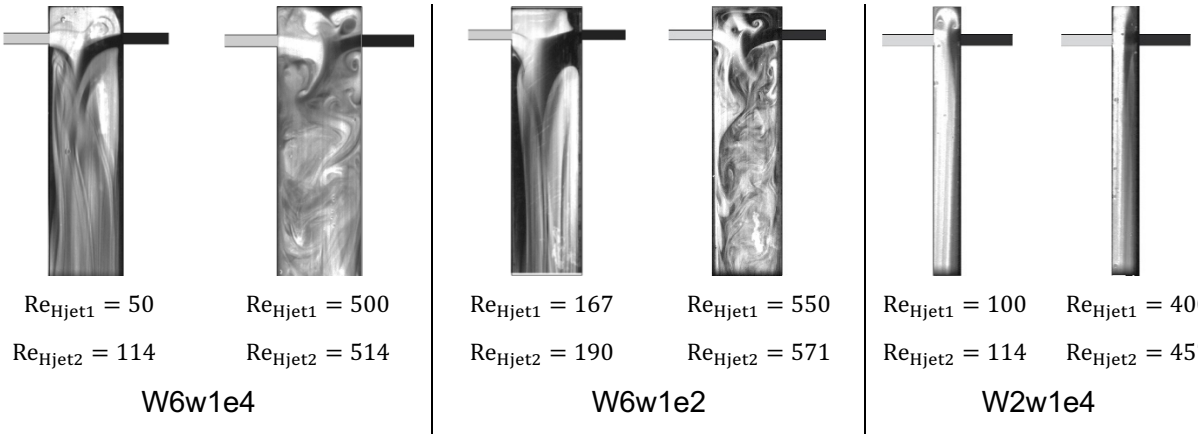

Figure 4. PLIF images in T-jets reactors W6w1e2, W6w1e4, and W2w1e4, for $\mu_1 = 1.7\ \mathrm{mPa \cdot s}$ (MV fluid) and $\mu_2 = 1.4\ \mathrm{mPa \cdot s}$ (MV fluid).

A larger viscosity ratio of $\mu_1/\mu_2 = 3$ was tested, and PLIF results for geometries W6w1e4 and W6w1e2 are shown in Figure 5. For this ratio, the W6w1e4 geometry is still able to develop a chaotic flow regime with strong mixing dynamics. PLIF images of the W6w1e4 mixer cover a narrow range of Reynolds numbers for jet 1, from $\mathrm{Re}_{\mathrm{Hjet1}} = 93$ to 136, where it is observed the onset of chaotic flow regime at $100 < \mathrm{Re}_{\mathrm{Hjet1}} < 136$. This transition for similar fluids occurs at a critical value of $\mathrm{Re}_{\mathrm{HJet}} \approx 100$. The highest viscosity jet seems to play a key role in the onset of the chaotic flow regime close to the critical value for similar fluids, although the value is decreased by around 30% due to the more unstable opposed jet at $\mathrm{Re}_{\mathrm{Hjet2}} > 600$.

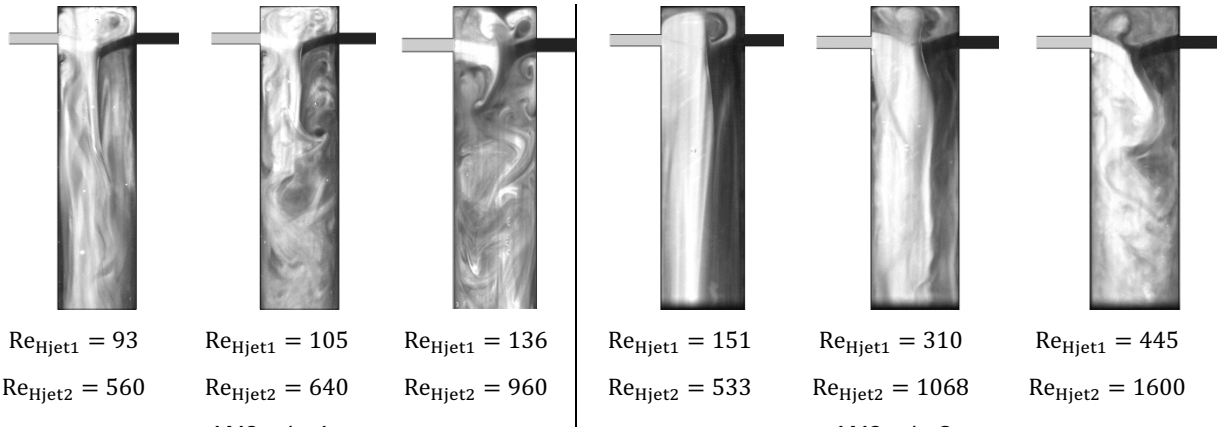

Figure 5. PLIF images in T-jets reactors W6w1e4 and W6w1e2, for $\mu_1 = 4.1\ \mathrm{mPa \cdot s}$ (MV fluid) and $\mu_2 = 1.4\ \mathrm{mPa \cdot s}$ (LV fluid).

PLIF images for the W6w1e2 geometry, where dynamic mixing is observed for similar fluids, are also shown in Figure 5. In this case, there is an onset of a dynamic flow regime at larger Reynolds numbers, and a clear chaotic flow regime is not observed, even for $\mathrm{Re}_{\mathrm{Hjet,MV}} \approx 445$.

Figures 4 and 5 show that the critical Reynolds number is defined by the MV fluid, which must also be $\mathrm{Re}_{\mathrm{HJet,MV}} > 100$, promoting the generation of a vortex street in the mixing chamber. Sultan et al. [20] also reported that the onset of self-sustainable chaotic flow regime for mixing of similar fluids occurs for Reynolds number above 100 for geometries with $W/w = 6$ and $W/e \geq 2$. The main results of this section are summarized in Table 2.

Table 2. Experimental conditions and detected transition Reynolds numbers

Case	Viscosity Ratio	Geometry	Transition $\mathrm{Re}_{\mathrm{Hjet}}$
0	1:1	*W6w1e4*	95-161
		W6w1e2	-
			-
1	1.2:1	*W6w1e4*	$\mathrm{Re}_{\mathrm{Hjet,LV}}: 343-514$ $\mathrm{Re}_{\mathrm{Hjet,MV}}: 300-500$
		W6w1e2	$\mathrm{Re}_{\mathrm{Hjet,LV}}: 190-381$ $\mathrm{Re}_{\mathrm{Hjet,MV}}: 167-333$
		W2w1e4	-
2	3:1	*W6w1e4*	$\mathrm{Re}_{\mathrm{Hjet,LV}}: 560-640$ $\mathrm{Re}_{\mathrm{Hjet,MV}}: 93-105$
		W6w1e2	$\mathrm{Re}_{\mathrm{Hjet,LV}}: 533-1067$ $\mathrm{Re}_{\mathrm{Hjet,MV}}: 151-310$

3.2 Effect of imbalance flow conditions on mixing of dissimilar fluids

From mixing studies on CIJs, it is known that the onset of chaotic flow regimes depends on the Reynolds number but also on the equilibrium of the opposed jets flow rates [26, 27]. Figure 6 shows a set of PLIF images for non-unitary flow rate ratios, r_s, for the T-jets geometry W6w1e4, which is the one where the chaotic flow regime occurs with the clearest features. The two opposed jets have the same viscosity, but jet 1 flow rates range from 20% to 84% ($0.20 \leq r_s \leq 0.84$) of jet 2 at $\mathrm{Re}_{\mathrm{Hjet2}} = 237$. Up to $r_s < 0.6$, the jet with the highest flow rate impinges in the opposed wall of the mixing chamber. At $r_s = 0.6$ the jets impingement point detaches from the wall, and there is the onset of vortex shedding. The dynamics of vortices formation is clearly observed as the jets flow rate ratio tends to one, and the impingement point converges to the mixing chamber plane symmetry.

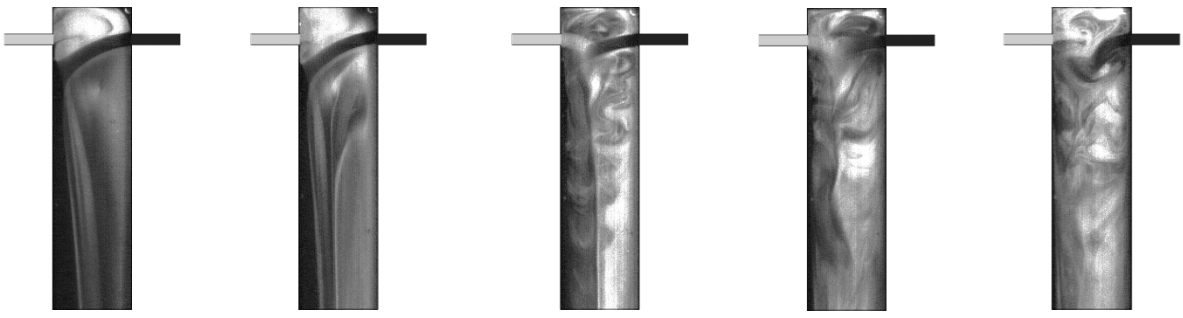

$\mathrm{Re}_{\mathrm{Hjet1}} = 47$ $\mathrm{Re}_{\mathrm{Hjet1}} = 95$ $\mathrm{Re}_{\mathrm{Hjet1}} = 142$ $\mathrm{Re}_{\mathrm{Hjet1}} = 190$ $\mathrm{Re}_{\mathrm{Hjet1}} = 199$

$r_s = 0.20$ $r_s = 0.40$ $r_s = 0.60$ $r_s = 0.80$ $r_s = 0.84$

Figure 6. PLIF images in T-jets reactors W6w1e4, for $\mu_1 = \mu_2 = 1.7\ \mathrm{mPa \cdot s}$ at $\mathrm{Re}_{\mathrm{Hjet2}} = 237$ and 47≤$\mathrm{Re}_{\mathrm{Hjet1}} \leq 199$.

The influence of the jets impact position on the flow regime is also assessed for non-unitary viscosity ratios in W6w1e4 (Figure 7). For $\mu_1/\mu_2 = 1.2$, jet 2 impinges on the mixing chamber wall for $r_s = 0.36$. When the jets flow rate ratio is $r_s = 0.71$, the impingement point is close to the mixing chamber plane symmetry. However, the flow regime is still below the onset of the chaotic flow regime. For $r_s = 1.1$ the impingement point is still around the chamber plane symmetry, and the flow regime is clearly chaotic. For $r_s = 1.4$, jet 1 impinges into the opposite wall, and the flow regime is clearly dynamic. The dynamic flow for $r_s = 1.4$ shows no vortex shedding, and thus this is not the fully developed chaotic flow regime reported for balanced jets.

Figure 7 also shows unbalanced conditions for the viscosity ratio of $\mu_1/\mu_2 = 3$. The jets impinge around the chamber plane symmetry in a range of $0.45 \leq r_s \leq 0.74$. When the more viscous jet $\mathrm{Re}_{\mathrm{Hjet,MV}} > 89$, the chaotic flow regime onsets. The chaotic flow regime occurs over a range of flow rate ratios, r_s, where one of the jets is not dominant to the point of impinging into the opposed wall. This principle is valid for viscosity ratios of at least up to 3. In sum, PLIF images in Figure 7 show the balance between jets occurs for a specific range of r_s (i.e. $0.71 < r_s < 1.4$ for $\mu_1/\mu_2 = 1.2$ and $0.45 < r_s < 0.74$ for $\mu_1/\mu_2 = 3$), not always promoting the chaotic mixing. This range is defined as a deviation of up to 30% from the equilibrium for both viscosity ratios. In CIJs, the range of flow rate ratios to equilibrate the jets is much tighter [26]. For example, at $\mathrm{Re} = 300$, a difference of 10% in r_s caused a decrease of twofold in the quality of mixing.

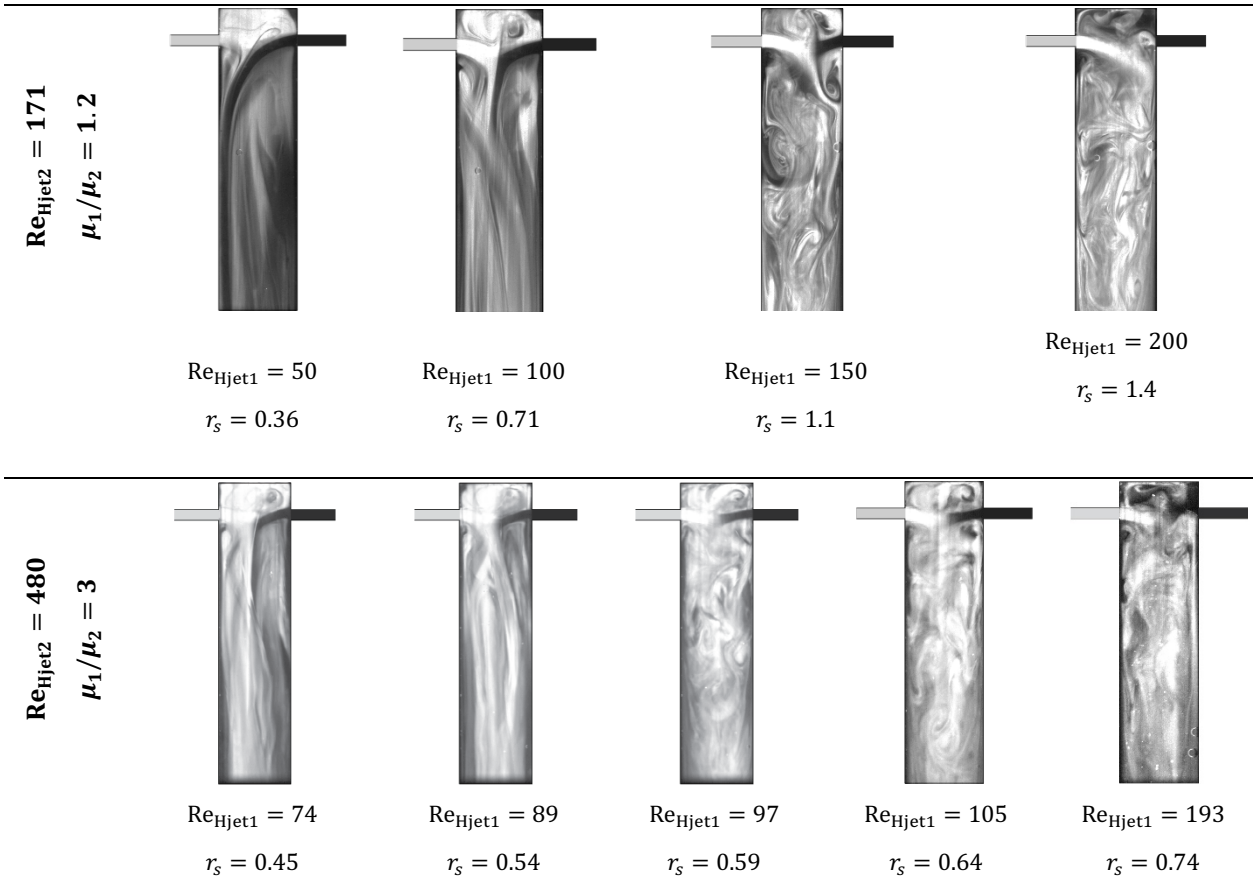

Figure 7. PLIF images in T-jets reactors W6w1e4, at different flow rate ratios, r_s, and two viscosity ratios: $\mu_1 = 1.7\ \mathrm{mPa \cdot s}$ (MV fluid) and $\mu_2 = 1.4\ \mathrm{mPa \cdot s}$ (LV fluid); and $\mu_1 = 4.1\ \mathrm{mPa \cdot s}$ (MV fluid) and $\mu_2 = 1.4\ \mathrm{mPa \cdot s}$ (LV fluid).

4 T-jets Design for Dissimilar Fluids

In T-jets, the impact point (IP) is not clear over the plane symmetry of the injectors. Both jets bend downwards, and the IP position is more affected downstream by r_s. Furthermore, the 3D movement of the flow makes the IP identification unclear. Here CFD simulations will be validated from PLIF data and will be used to determine the position of the IP.

4.1 CFD model

3D CFD simulations of T-jets flow dynamics were performed using ANSYS/Fluent. The physical domain and the respective dimensions are those represented in Figure 1 for W6w1e4 geometry. Steady-state laminar flow was simulated by solving the following set of mass and conservation equations,

$$\nabla \cdot (\rho \mathbf{u}) = 0 \tag{3}$$

$$\nabla \cdot (\rho \mathbf{u}\mathbf{u}) = -\nabla p + \nabla \cdot [\mu(\nabla \mathbf{u} + \nabla \mathbf{u}^{\mathrm{T}})] + \rho \mathbf{g} \tag{4}$$

where $\mathbf{u}$ is the velocity field, p is the pressure, and $\mathbf{g}$ is the gravity acceleration, μ and ρ are the viscosity and density of fluids, respectively. A similar modelling of mixing of two incompressible miscible fluids is under analysis in Joseph et al. [34]. The convergence criterion for the residuals, in this work, is 10^{-6}. For flow simulation, the SIMPLE scheme was used for pressure-velocity coupling, and for spatial discretization, Least Squares Cell based is used as gradient solver. A Second Order discretization scheme was used for pressure, and Second Order Upwind for momentum.

The consideration of two dissimilar fluids requires the simulation of the mass transfer using

$$\frac{\mathbf{D}C}{\mathbf{D}t} = D_m(C)\nabla^2 C \tag{5}$$

where C is the concentration of species, which can correspond to the liquid injected through injector 1 or 2 and D_m is the molecular diffusivity. $D_m = 1 \times 10^{-9}\ \mathrm{m^2\ s^{-1}}$ was used in the simulations. The mass transfer equation was solved in CFD simulations using Second-Order Upwind solver. The mixture viscosity and density were described by the mass-weighted mixing and the volume-weighted mixing laws,

$$\mu = \omega_g \mu_g + \omega_w \mu_w \tag{6}$$

$$\rho = \phi_g \rho_g + \phi_w \rho_w \tag{7}$$

where ω_g and ω_w are the mass fraction and ϕ_g and ϕ_w are volume fraction of glycerol and water, respectively.

The boundary conditions were set as uniform and constant pressure at the outlet and no-slip conditions at the walls. At inlet 1, the velocity is $\mathbf{u} = (v_{\mathrm{inj1}}, 0,0)$, and at inlet 2, the velocity is $\mathbf{u} = (-v_{\mathrm{inj2}}, 0,0)$. The inlet conditions have a great impact on the flow dynamics, and thus the injectors are 15 mm long to ensure a fully developed flow regime at the mixing chamber entrance [35]. The grid independence for this geometry was reported in Sultan et al. [33]. It is demonstrated from monitoring the velocity at outlet that geometry with 20×10^3 elements is enough to describe the main flow features. Sultan et al. [12] also validated the mesh and CFD model for the simulation of the dynamic flow regimes from experimental results. Nevertheless, the simulation domain was discretized with uniformly sized cubic finite volumes with 0.25 mm length sides, which makes a total of 50×10^3 cells. CFD simulations are only used in this work to determine the impingement point position in the mixing chamber, and not the mixing dynamics and quality, which requires more accuracy regarding the simulation of mass transfer scales in the mixing chamber. These simulations were also validated from comparison with PLIF results.

4.2 Results

Figure 8 shows PLIF images and CFD results for W6w1e4 at $\mathrm{Re_{Hjet2}} = 80$. The CFD pathlines cover a range of flow rate ratios $0.8 \leq r_s \leq 1.2$. The physical properties of fluids set in CFD simulations are: $\mu_1/\mu_2 = 1$, $\rho = 996\ \mathrm{kg\ m^{-3}}$, and $\mu = 8.89 \times 10^{-4}\ \mathrm{Pa \cdot s}$. The streamlines issuing from injector 1 are represented in grey, and the opposite injector streamlines are in black. CFD results were compared with PLIF images for the same conditions.

Deviations of impinged jets in experiments can be estimated from the comparison between PLIF images and the pathlines. At the range of flow rates for $\mathrm{Re_{Hjet2}} = 80$, the deviation from the set point of the flow controllers is up to 10% (5% on each side). This deviation is mainly due to the fabrication technique, CNC milling, that has a tolerance of 50 μm. The 10% is the worst-case-scenario that assumes maximum deviation of the opposite nozzles' width having opposite signs. Therefore, symmetric flow conditions visualized from experiments correspond to $0.9 \leq r_s \leq 1.1$ obtained from CFD simulations. The PLIF images are in good agreement with the pathlines in this range.

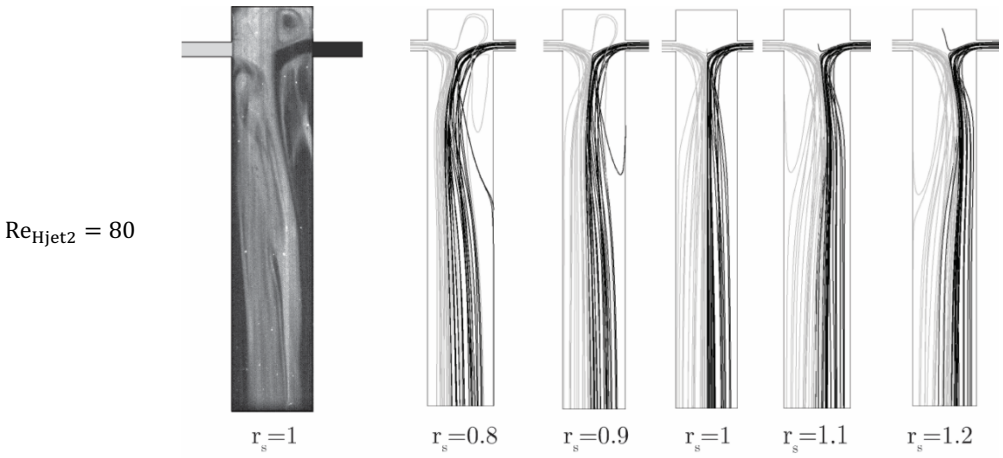

Figure 8. PLIF image and streamlines for different flow rate ratios r_s for mixing of two fluids with the same physical properties and using the geometry W6w1e4.

Two main conclusions can be drawn from the CFD results. The first is the more accurate control of the flow conditions in simulations. The second is that the deviations from symmetry conditions are clear at downstream positions from the jets. Thus, the position of the contact point between both jets was determined over a line normal to the mixing chamber plane symmetry and positioned at a distance equal to $W = 6\ \mathrm{mm}$ from the injectors' plane symmetry, as showed in Figure 9. Over this line, the local maximum of the velocity profile is related to the IP. Hereafter, the IP of the jets is obtained from this method.

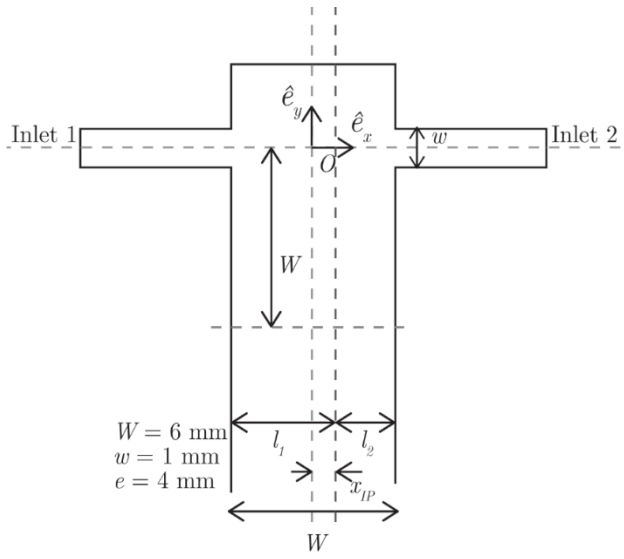

Figure 9. Sketch of an axial cut of the T-Jet mixing chamber and representation of the position to determine the impingement point from CFD simulations.

Figure 10 shows the IP obtained from CFD simulations for W6w1e4, keeping constant the Reynolds number of the more viscous fluid, $\mathrm{Re}_{\mathrm{Hjet2}} = 50$, and using three viscosities ratios, 1 (Case 3), 2 (Case 4) and 3 (Case 5), as described in Table 3. The Reynolds number of the opposite injector, $\mathrm{Re}_{\mathrm{Hjet1}}$, was changed and the IP was determined from CFD results. The IP dimensionless position (ξ) is defined in terms of normalized distance to the axial position (x_{IP})

$$\xi = \frac{x_{\mathrm{IP}}}{W/2} \tag{8}$$

For similar fluids $(\mu_1/\mu_2 = 1)$, IP is at the axial position when the flow rates are matched: $\mathrm{Re}_{\mathrm{Hjet1}} = \mathrm{Re}_{\mathrm{Hjet2}} = 50$, and $r_s = 1$. For dissimilar viscosities, Figure 10 shows that the equilibrium also at $r_s = 1$, which corresponds to $\mathrm{Re}_{\mathrm{Hjet1}}\colon \mathrm{Re}_{\mathrm{Hjet2}} = 27\colon 50$ when $\mu_1/\mu_2 = 1.2$, and to $\mathrm{Re}_{\mathrm{Hjet1}}\colon \mathrm{Re}_{\mathrm{Hjet2}} = 17\colon 50$ when $\mu_1/\mu_2 = 3$. When the flow rate of one jet deviates from the equilibrium more than

50%, the IP gets too close to the mixing chamber walls. This blocks the onset of chaotic flow regimes, as shown from PLIF data.

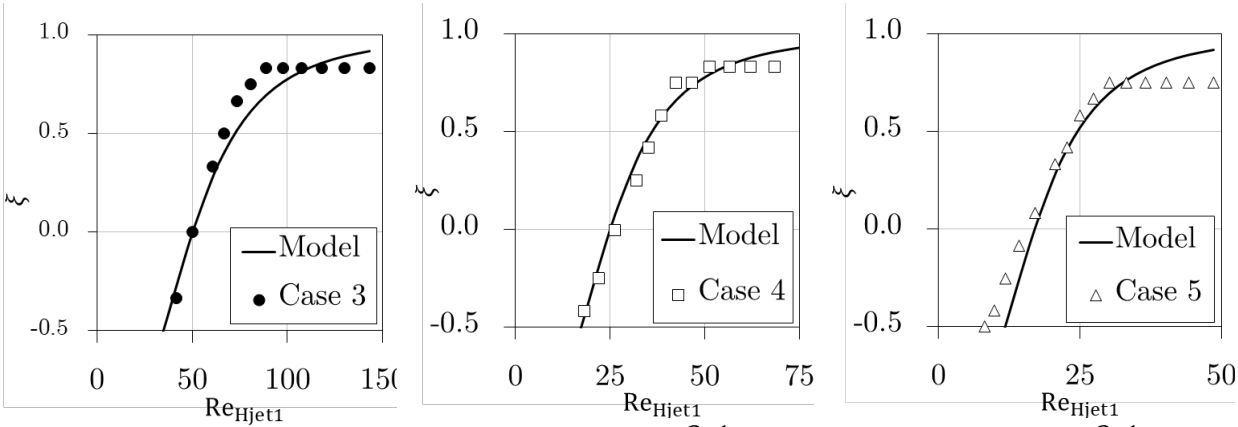

Figure 10. Non-dimensional impingement point position from CFD simulations of the T-jets geometry W6w1e4, for $0.5 < r_s < 3$ at $\mathrm{Re}_{\mathrm{Hjet2}} = 50$.

Table 3. Sets of fluids for mixing experiments in T-Jets

Case	Viscosity Ratio	μ	ρ	$\mathrm{Re}_{\mathrm{MV}}$
3	1	$1\ \mathrm{mPa \cdot s}$	$998\ \mathrm{kg\ m^{-3}}$	50
4	2	$\mu_{\mathrm{MV}} = 40\ \mathrm{mPa \cdot s}$ $\mu_{\mathrm{LV}} = 20\ \mathrm{mPa \cdot s}$	$\rho_{\mathrm{MV}} = 1208\ \mathrm{kg\ m^{-3}}$ $\rho_{\mathrm{LV}} = 1176\ \mathrm{kg\ m^{-3}}$	50
5	3	$\mu_{\mathrm{MV}} = 4.1\ \mathrm{mPa \cdot s}$ $\mu_{\mathrm{LV}} = 1.4\ \mathrm{mPa \cdot s}$	$\rho_{\mathrm{MV}} = 1105\ \mathrm{kg\ m^{-3}}$ $\rho_{\mathrm{LV}} = 1257\ \mathrm{kg\ m^{-3}}$	50

4.3 Design Equation

The jets balance when the flow rates match, regardless of viscosity ratio. This fact raises the possibility that the IP location is governed by the kinetic energy ratio of the two opposite forces. A model that describes the IP position is developed based on the jets' kinetic energy rate balance [4] [26]. The kinetic energy rate balance (KEB) model assumes that both jets behave as springs in equilibrium. Each jet exerts a force proportional to the horizontal distance between said jet nozzle and the IP, i.e., the force exerted by jet 1 over jet 2 is $F_{1\to2} = Kl_1$, where K is Hooke's law constant and l_1 is the horizontal distance from the IP to the wall from where jet 1 issues. Conversely, the force exerted by jet 2 on jet 1 is: $F_{2\to1} = Kl_2$. When the two forces are balanced $F_{1\to2} = F_{2\to1}$ and so $F_{1\to2}/F_{2\to1} = Kl_1/Kl_2$. Fonte et al. [26] demonstrated for CIJs that the kinetic energy rate of the opposed jets, $\dot{E_K}$, is proportional to the potential energy stored in the spring, which gives

$$\frac{\dot{E_{K1}}}{\dot{E_{K2}}} = \frac{l_1}{l_2} \tag{9}$$

where the ratio of kinetic energy rate for two jets issuing from equal nozzles is given by

$$\frac{\dot{E_{K1}}}{\dot{E_{K2}}} = \frac{\rho_1 v_1^3}{\rho_2 v_2^3} = \frac{l_1}{l_2} \tag{10}$$

and v is the space averaged velocity at each nozzle. According to Figure 9, the length l can be related to the IP location (x_{IP}) in relation to the mixing chamber plane symmetry as

$$\begin{cases} l_1 = \frac{W}{2} + x_{\mathrm{IP}} \\ l_2 = \frac{W}{2} - x_{\mathrm{IP}} \end{cases} \quad (11)$$

Combining Equation 10 with Equation 11, and considering the definition of ξ, the dimensionless IP is given by

$$\xi = \frac{\frac{\rho_1 v_1^3}{\rho_2 v_2^3} - 1}{\frac{\rho_1 v_1^3}{\rho_2 v_2^3} + 1} \quad (12)$$

This equation describes the position of the impingement point in the mixing chamber and only takes into account the ratios of density and inlet velocities. Equation 12 is represented in the results of Figure 10 with the name model in the legend, enabling the comparison with the IP determined from CFD simulations for viscosity ratios of 1, 2 and 3. The simulated cases only considered symmetric nozzles and, the model is assessed for the flow rate ratios and viscosity ratios in the range: $1 \leq r_s \leq 3$ and $1 \leq \mu_1/\mu_2 \leq 3$. Results in Figure 10 indicate the validation of the KEB model (Equation 12) from CFD simulation results.

The viscosity ratios in the tested range show no influence on the design of mixing conditions in T-jets. This differs from CIJs, where the jets are round and expand in the mixing chamber asymmetrically depending on viscosity, as described by the Narrow Axisymmetric Jet model [26]. Therefore, mixing in T-jets is less sensitive to differences in viscosity comparing to CIJs.

The validation of this model makes it a tool to design T-Jets mixers for industrial processes. Results in this work show that the onset of chaotic flow regime in T-Jets mixers occurs for $\xi = 0$ and $\mathrm{Re}_{\mathrm{HJet,MV}} > 100$, and so the conditions of the opposed jets can be determined from Equation 12 imposing these conditions.

5 Conclusions

The operation at chaotic flow regimes was demonstrated and studied, for the first time, in T-jets mixers for mixing of dissimilar fluids. The key conditions for the onset of the self-sustainable chaotic flow regimes are: the critical Reynolds number is set by the more viscous jet stream and must be $\mathrm{Re}_{\mathrm{HJet}} > 100$; and the opposed inlet jets must be well-balanced and impinged at the mixing chamber plane symmetry. These conditions were set from PLIF results using fluids with a viscosity ratio between 1.2 and 3, and then validated from CFD simulations. A model to predict the IP location is proposed for the design of T-jets over a wide range of jet flow rate ratios and validated from CFD simulations. This model can be used to design T-jets for the mixing of dissimilar fluids by setting $\xi = 0 \text{ and } \mathrm{Re}_{\mathrm{HJet,MV}} > 100$.

Acknowledgement

This work was financially supported by: Base-UIDB/50020/2020 and Programmatic-UIDP/50020/2020 Funding of LSRE-LCM, funded by national funds through FCT/MCTES (PIDDAC) and by POCI-01-0145-FEDER-030445 – funded by European Regional Development Fund (ERDF) - Programa Operacional Competitividade e Internacionalização (POCI) – and by national funds through FCT - Fundação para a Ciência e a Tecnologia IP; Margarida S.C. A. Brito acknowledges her FCT scholarship PD/BD/135060/2017.

Symbols used

d_{Hjet} – hydraulic diameter of the inlet channel

e – depth of the T-jet mixer

$\dot{E}_{Ki}$ – kinetic energy rate of jet i

H – height of the mixing chamber of the T-jet mixer

l_i – horizontal distance from the impingement point position to the wall where jet i issues

p – pressure

q_i – flow rate at inlet channel i

r_s – ratio between the flow rate of the opposed jets

$\mathrm{Re}_{\mathrm{Hjet}}$ – hydraulic Reynolds number

$\mathrm{Re}_{\mathrm{Hjet1}}$ – hydraulic Reynolds number at jet 1

$\mathrm{Re}_{\mathrm{Hjet2}}$ – hydraulic Reynolds number at jet 2

v_i – velocity of jet i

$\mathbf{u}$ – velocity vector

x – position according to the jets direction

x_{IP} – impingement point position

w – width of the inlet channels of the T-jet mixer

W – width of the mixing chamber of the T-jet mixer

Greek letters

μ – viscosity

ξ – dimensionless IP position

ρ – density

v_{inj} – surface velocity at inlet channel

ϕ – volume fraction

ω – mass fraction

Sub- and Superscripts

1, 2 – inlet channel 1 or 2, respectively

Abbreviations

IP – Impact Point of the opposed jets

KEB – Analytical model based on kinetic energy rate balance

PLIF - Planar Laser Induced Fluorescence

References

[1] D. Gobby, P. Angeli, A. Gavriilidis. *J. Micromech. Microeng.*, **2001**, *11*(*2*), 126-32 DOI: 10.1088/0960-1317/11/2/307.

[2] M. Engler, N. Kockmann, T. Kiefer, P. Woias. *Chem. Eng. J.*, **2004**, *101*(*1-3*), 315-322 DOI: 10.1016/j.cej.2003.10.017.

[3] S.H. Wong, M.C.L. Ward, C.W. Wharton. *Sensor. Actuat. B-Chem.*, **2004**, *100*, 359-379 DOI: 10.1016/j.snb.2004.02.008.

[4] D. Bothe, C. Stemich, H.-J. Warnecke. *Chem. Eng. Sci.*, **2006**, *61*(*9*), 2950-2958 DOI: 10.1016/j.ces.2005.10.060.

[5] M. Hoffmann, M. Schlüter, N. Räbiger. *Chem. Eng. Sci.*, **2006**, *61*(*9*), 2968-2976 DOI: 10.1016/j.ces.2005.11.029.

[6] A. Soleymani, E. Kolehmainen, I. Turunen. *Chem. Eng. J.*, **2007**, *135*(*SUPPL. 1*), S219-S228 DOI: 10.1016/j.cej.2007.07.048.

[7] D. Bothe, A. Lojewski, H.-J. Warnecke. *AIChE J.*, **2010**, *56*(*6*), 1406-1415 DOI: 10.1002/aic.12067.
[8] S. Thomas, T. Ameel, J. Guilkey. *Phys. Fluids*, **2010**, *22*(*1*), 013601 DOI: 10.1063/1.3283063.
[9] S. Thomas, T.A. Ameel. *Exp. Fluids*, **2010**, *49*(*6*), 1231-1245 DOI: 10.1007/s00348-010-0863-7.
[10] A. Mariotti, C. Galletti, R. Mauri, M.V. Salvetti, E. Brunazzi. *Chem. Eng. J.*, **2018**, *341*, 414-431 DOI: 10.1016/j.cej.2018.01.108.
[11] J.-W. Zhang, S.-F. Liu, C. Cheng, W.-F. Li, X.-L. Xu, H.-F. Liu, F.-C. Wang. *Chem. Eng. J.*, **2019**, *358*, 1561-1573 DOI: 10.1016/j.cej.2018.10.112.
[12] W.-F. Li, T.-L. Yao, H.-F. Liu, F.-C. Wang. *AIChE J.*, **2011**, *57*(*6*), 1434-1445 DOI: 10.1002/aic.12369.
[13] T. Schikarski, W. Peukert, M. Avila. *Chem. Eng. J.*, **2017**, *324*, 168-181 DOI: 10.1016/j.cej.2017.04.119.
[14] G. Orsi, M. Roudgar, E. Brunazzi, C. Galletti, R. Mauri. *Chem. Eng. Sci.*, **2013**, *95*, 174-183 DOI: 10.1016/j.ces.2013.03.015.
[15] G. Orsi, C. Galletti, E. Brunazzi, R. Mauri. *Chem. Engineer. Trans.*, **2013**, *32*, 1471-1476 DOI: 10.3303/CET1332246.
[16] C. Galletti, E. Brunazzi, R. Mauri. *Chem. Eng. Sci.*, **2017**, *164*, 333-343 DOI: 10.1016/j.ces.2017.02.035.
[17] A.A. Thorat, S.V. Dalvi. *Chem. Eng. J.*, **2012**, *181-182*, 1-34 DOI: 10.1016/j.cej.2011.12.044.
[18] T. Schikarski, H. Trzenschiok, M. Avila, W. Peukert. *Chem. Eng. Technol.*, **2019**, DOI: 10.1002/ceat.201900095.
[19] J. Gradl, H.-C. Schwarzer, F. Schwertfirm, M. Manhart, W. Peukert. *Chem. Eng. Process*, **2006**, *45*(*10*), 908-916 DOI: 10.1016/j.cep.2005.11.012.
[20] M.A. Sultan, C.P. Fonte, M.M. Dias, J.C.B. Lopes, R.J. Santos. *Chem. Eng. Sci.*, **2012**, *73*, 388-399 DOI: 10.1016/j.ces.2012.02.010.
[21] M.A. Sultan, K. Krupa, C.P. Fonte, M.I. Nunes, M.M. Dias, J.C.B. Lopes, R.J. Santos. *Chem. Eng. Technol.*, **2013**, *36*(*2*), 323-331 DOI: 10.1002/ceat.201200141.
[22] G.-Y. Tu, W.-F. Li, K.-J. Du, F.-C. Wang. *Chem. Eng. Sci.*, **2014**, *116*, 734-744 DOI: 10.1016/j.ces.2014.06.003.
[23] G.-Y. Tu, W.-F. Li, W.-W. Qian, Z.-H. Shi, H.-F. Liu, F.-C. Wang. *Chem. Eng. Sci.*, **2015**, *134*, 67-75 DOI: 10.1016/j.ces.2015.04.048.
[24] K. Krupa, M.I. Nunes, R.J. Santos, J.R. Bourne. *Chem. Eng. Sci.*, **2014**, *111*, 48-55 DOI: 10.1016/j.ces.2014.02.018.
[25] K. Krupa, M.A. Sultan, C.P. Fonte, M.I. Nunes, M.M. Dias, J.C.B. Lopes, R.J. Santos. *Chem. Eng. J.*, **2012**, *207-208*, 931-937 DOI: 10.1016/j.cej.2012.07.062.
[26] C.P. Fonte, M.A. Sultan, R.J. Santos, M.M. Dias, J.C.B. Lopes. *AIChE J.*, **2016**, *62*(*6*), 2200-2212 DOI: 10.1002/aic.15169.
[27] C.P. Fonte, M.A. Sultan, R.J. Santos, M.M. Dias, J.C.B. Lopes. *Chem. Eng. J.*, **2015**, *260*, 316-330 DOI: 10.1016/j.cej.2014.08.090.
[28] M.S.C.A. Brito, L.P. Esteves, C.P. Fonte, M.M. Dias, J.C.B. Lopes, R.J. Santos. *Chem. Eng. Res. Des.*, **2018**, *134*, 392-404 DOI: 10.1016/j.cherd.2018.04.020.
[29] R.J. Santos, M.A. Sultan. *Chem. Eng. Technol.*, **2013**, *36*(*6*), 937-949 DOI: 10.1002/ceat.201200678.
[30] W.F. Li, T.L. Yao, F.C. Wang. *AIChE J.*, **2010**, *56*(*10*), 2513-2522 DOI: 10.1002/aic.12188.
[31] J.-W. Zhang, W.-F. Li, X.-L. Xu, M. El Hassan, H.-F. Liu, F.-C. Wang. *Chem. Eng. J.*, **2020**, *387*, DOI: 10.1016/j.cej.2020.124148.
[32] W. Zhang, J.-W. Zhang, W.-F. Li, H.-F. Liu, F.-C. Wang. *Chem. Eng. Sci.*, **2020**, *228*, DOI: 10.1016/j.ces.2020.115991.
[33] M.A. Sultan, S.L. Pardilhó, M.S.C.A. Brito, C.P. Fonte, M.M. Dias, J.C.B. Lopes, R.J. Santos. *Chem. Eng. Technol.*, **2019**, *42*(*1*), 119-128 DOI: 10.1002/ceat.201700684.
[34] D.D. Joseph, A. Huang, H. Hu. *Physica D*, **1996**, *97*(*1*), 104-125 DOI: 10.1016/0167-2789(96)00097-8.

[35] C. Galletti, M. Roudgar, E. Brunazzi, R. Mauri. *Chem. Eng. J.*, **2012**, *185-186*, 300-313 DOI: 10.1016/j.cej.2012.01.046.

Table and Figure captions

Table 1. Sets of fluids for mixing experiments in T-Jets.

Table 2. Experimental conditions and detected transition Reynolds numbers.

Table 3. Sets of fluids for mixing experiments in T-Jets.

Figure 1. T-jets experimental set-up and mixer geometry.

Figure 2. Variation of refractive index and viscosity with the mass fraction of $CaCl_2$.

Figure 3. PLIF images in T-jets reactors W6w1e2 and W6w1e4, for $\mu_1 = \mu_2 = 1.7\ \mathrm{mPa \cdot s}$.

Figure 4. PLIF images in T-jets reactors W6w1e2, W6w1e4, and W2w1e4, for $\mu_1 = 1.7\ \mathrm{mPa \cdot s}$ (MV fluid) and $\mu_2 = 1.4\ \mathrm{mPa \cdot s}$ (MV fluid).

Figure 5. PLIF images in T-jets reactors W6w1e4 and W6w1e2, for $\mu_1 = 4.1\ \mathrm{mPa \cdot s}$ (MV fluid) and $\mu_2 = 1.4\ \mathrm{mPa \cdot s}$ (LV fluid).

Figure 6. PLIF images in T-jets reactors W6w1e4, for $\mu_1 = \mu_2 = 1.7\ \mathrm{mPa \cdot s}$. at $\mathrm{Re}_{\mathrm{Hjet2}} = 237$ and $47 \leq \mathrm{Re}_{\mathrm{Hjet1}} \leq 199$.

Figure 7. PLIF images in T-jets reactors W6w1e4, at different flow rate ratios, r_s, and two viscosity ratios: $\mu_1 = 1.7\ \mathrm{mPa \cdot s}$ (MV fluid) and $\mu_2 = 1.4\ \mathrm{mPa \cdot s}$ (LV fluid); and $\mu_1 = 4.1\ \mathrm{mPa \cdot s}$ (MV fluid) and $\mu_2 = 1.4\ \mathrm{mPa \cdot s}$ (LV fluid).

Figure 8. PLIF image and streamlines for different flow rate ratios r_s for mixing of two fluids with the same physical properties and using the geometry W6w1e4.

Figure 9. Sketch of an axial cut of the T-Jet mixing chamber and representation of the position to determine the impingement point from CFD simulations.

Figure 10. Non-dimensional impingement point position from CFD simulations of the T-jets geometry W6w1e4, for $0.5 < r_s < 3$ at $\mathrm{Re}_{\mathrm{Hjet2}} = 50$